The antiferromagnetic to ferrimagnetic phase transition in $Mn_2Sb_{1-x}Bi_x$ compounds

Shen, Qi; Batashev, Ivan; Zhang, Fengqi; Ojiyed, Hamutu; van Dijk, Niels; Brück, Ekkes

DOI
10.1016/j.jallcom.2021.158963

Publication date
2021

Document Version
Final published version

Published in
Journal of Alloys and Compounds

Journal of Alloys and Compounds 866 (2021) 158963

Contents lists available at ScienceDirect

Journal of Alloys and Compounds

journal homepage: www.elsevier.com/locate/jalcom

The antiferromagnetic to ferrimagnetic phase transition in $Mn_2Sb_{1-x}Bi_x$ compounds

Qi Shen*, Ivan Batashev, Fengqi Zhang, Hamutu Ojiyed, Niels van Dijk, Ekkes Brück

Fundamental Aspects of Materials and Energy, Faculty of Applied Sciences, Delft University of Technology, Mekelweg 15, 2629 JB Delft, The Netherlands

ARTICLE INFO

Article history:
Received 21 October 2020
Received in revised form 15 January 2021
Accepted 26 January 2021
Available online 30 January 2021

Keywords:
Inverse magnetocaloric effect
Antiferro-to-ferrimagnetic phase transition
Exchange inversion

ABSTRACT

The influence of partial substitution of Bi for Sb on the structure, magnetic properties and magnetocaloric effect of $Mn_2Sb_{1-x}Bi_x$ (x = 0, 0.02, 0.04, 0.05, 0.07, 0.09, 0.15, 0.20) compounds has been investigated. The transition temperature of the antiferro-to-ferrimagnetic (AFM-FIM) transition initially increases with increasing Bi and decreases above 9%. Density functional theory calculations indicate that the Bi atoms prefer to occupy only the Sb site, which accounts for the large magnetization jump in $Mn_2Sb_{0.93}Bi_{0.07}$. As large lattice parameters are found for Bi substituted Mn_2Sb, the origin of the AFM-FIM transition in $Mn_2Sb_{(1-x)}Bi_x$ compounds is ascribed to an enhanced coefficient of thermal expansion along the c axis, resulting from the Bi substitution. The moderate entropy change of 1.17 J/kg K under 2 T originating from the inverse magnetocaloric effect and the strong magnetic field dependence of the transition temperature of $dT_t/d\mu_0 H$ = −5.4 K/T in $Mn_2Sb_{0.95}Bi_{0.05}$ indicate that this alloy is a promising candidate material for magnetocaloric applications.

1. Introduction

Magnetic refrigeration and waste heat recovery are environmentally-friendly technological applications based on the magnetocaloric effect (MCE) [1,2]. MCE can be characterized by an isothermal entropy change or an adiabatic temperature change when the material is exposed to a change in external magnetic field. Most giant MCE materials present a large MCE at an order-disorder transition accompanied with a change in symmetry (with a large volume change), as found in Gd-Si-Ge [3], MnAs [4] and Ni-Mn-based Heusler alloys [5], or an order-disorder transition without a change in symmetry, as found in La-Fe-Si [6] and Mn-Fe-P [7], which show a discontinuous change in lattice constants (with a small volume change). For MCE materials with an order-disorder transition, a large thermal or magnetic hysteresis can occur, which is detrimental for cyclic magnetocaloric applications. On the other hand, order-order transitions, such as an antiferro-to-ferromagnetic [5] or antiferro-to-ferrimagnetic (AFM-FIM) transition [8] can also present large magnetic entropy change with discontinuous lattice constants. These materials are easier to achieve almost free of hysteresis and a high sensitivity of the magnetization with temperature [3,8].

In Mn_2Sb-based alloys an AFM-FIM order-order transition has been reported. The Mn_2Sb-based compound is an intermetallic compound, which is low cost, easy to prepare and nontoxic. The binary Mn_2Sb compound crystallizes in a tetragonal Cu_2Sb-type structure (space group $P4/nmm$) with a Curie temperature (T_C) of 550 K [9]. The magnetic moments are mainly attributed to the Mn atoms, which are positioned at two different crystallographic sites, Mn-I (2a) and Mn-II (2c), stacked antiparallel in triple layers. Neutron diffraction indicated that the Mn-I and Mn-II atoms possess 2.1 and −3.9 μ_B, respectively [9]. The repeated stacking of Mn-II /Mn-I /Mn-II leads to the ferrimagnetic ordering below 550 K [10]. Upon cooling, the moments of Mn-I and Mn-II both reorient from being parallel to the c axis of tetragonal lattice into the a-b basal plane at a temperature of about 240 K, which has been identified as the spin reorientation temperature (T_{SR}). Upon further cooling, a FIM-AFM transition has been reported in ternary compounds for substitution of Mn with Cu [11], Cr [8], Zn [12], Co [13] or for substitution of Sb with Ge [14], Sn [15], and As [16]. An overview of different substitutions in Mn_2Sb can be found in a recent review of Caron [17]. The reported AFM ordering shows an anti-parallel arrangement of adjacent Mn-II moments along the c axis [13]. The basic mechanism behind the AFM-FIM transition is based on the exchange inversion initially proposed by Kittel [18]. The reduced lattice constant c by the introduction of smaller atoms decreases the distance of adjacent Mn-II atoms, which triggers exchange inversion by the normal thermal contraction.

* Corresponding author.
E-mail address: q.shen@tudelft.nl (Q. Shen).

https://doi.org/10.1016/j.jallcom.2021.158963
0925-8388/

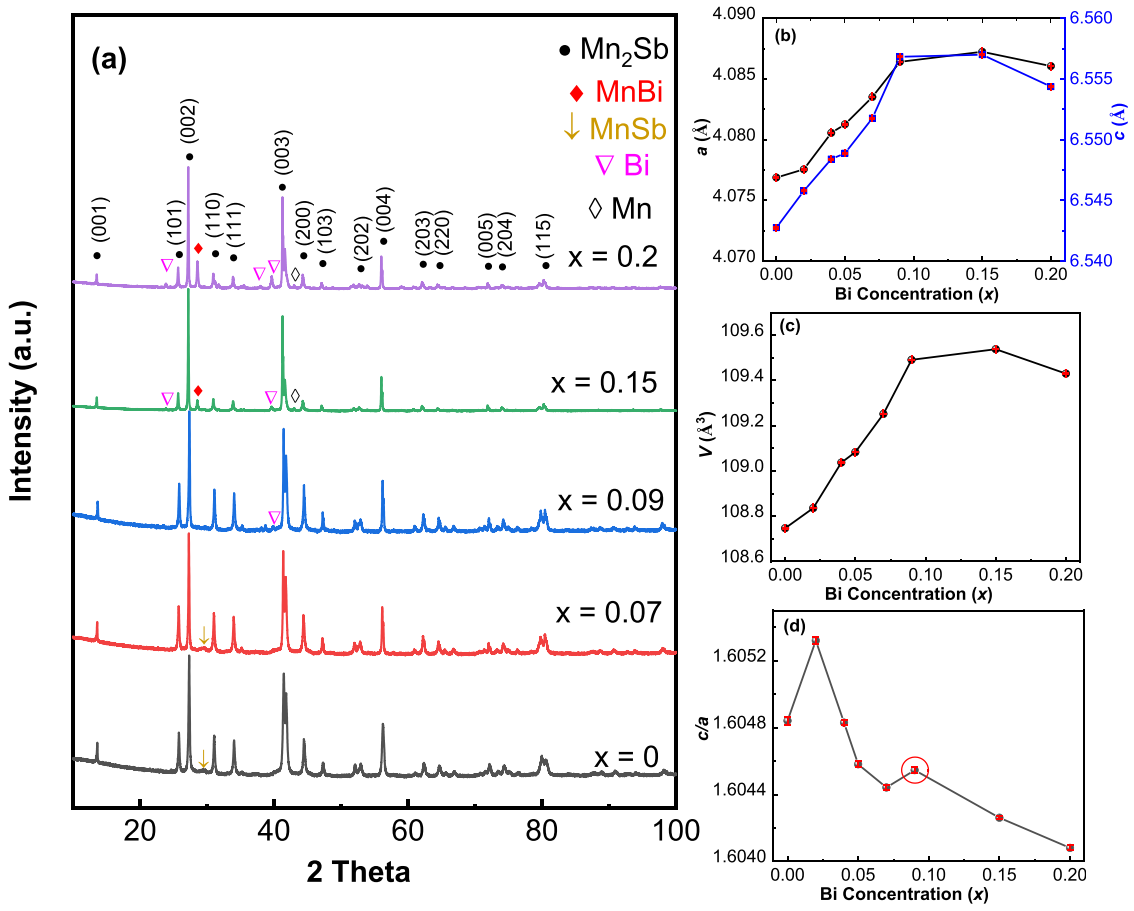

Fig. 1. (a) XRD patterns, (b) lattice parameters *a* and *c*, (c) unit-cell volume *V*, (d) the ratio of *c*/*a* derived from XRD as a function of the Bi concentration for $Mn_2Sb_{1-x}Bi_x$ (x = 0, 0.02, 0.04, 0.05, 0.07, 0.09, 0.15, 0.20). The red circle marks the turning point of *c*/*a* at x = 0.09. For clarity of presentation, the patterns for x = 0.02, 0.04 and 0.05 are omitted because of their close similarity to the patterns for x = 0 and 0.07. (For interpretation of the references to colour in this figure legend, the reader is referred to the web version of this article.)

Interestingly, this AFM-FIM transition was also reported in larger atom Bi doped Mn_2Sb [19,20]. Ohshima el al. [19] found a large magnetization jump around 100–140 K in $(Mn_2Sb)_{0.89}Bi_{0.11}$ and Zhang el al. [20] discussed the role of Bi-rich grain boundary precipitates (that were found to coat the main phase) on the magnetic transition. However, few studies focused on how Bi substitution for Sb influences the magnetic properties. Therefore, this paper aims to study the structure, magnetic properties and MCE in arc-melted $Mn_2Sb_{1-x}Bi_x$ (x = 0, 0.02, 0.04, 0.05, 0.07, 0.09, 0.15, 0.20) compounds.

2. Experimental methods

Polycrystalline $Mn_2Sb_{1-x}Bi_x$ (x = 0, 0.02, 0.04, 0.05, 0.07, 0.09, 0.15, 0.20) compounds were prepared from high purity elements (Mn 99.9%, Bi 99.99%, Sb 99.5%) by arc melting. Then the arc-melted samples were annealed for homogenization under argon atmosphere at 1073 K for 16 h followed by quenching into water. X-ray diffraction (XRD) data were collected with a Panalytical X-Pert PRO using Cu-Kα radiation and an Anton Paar TTK 450 temperature chamber. Lattice constants were analysed by Rietveld refinement using Fullprof (see Fig. S1 in the Supplementary Material) [21]. The microstructure was analysed by the Scanning Electron Microscopy (SEM, JEOL JSM IT100LA) equipped with the Energy Dispersive X-ray Spectroscopy (EDS). The low-temperature magnetic properties were measured on a superconducting quantum interference device (SQUID) magnetometer model MPMS-XL, equipped with the reciprocating sample option. High-temperature magnetic measurements were carried out using a vibrating sample magnetometer (VSM) model LakeShore 7307 equipped with a high-temperature oven (model 73034). Magnetization-temperature (*M-T*) curves were conducted with zero-field cooled (ZFC), field heated (FH) and field cooled (FC) protocols. Due to the mixed magnetic states at low temperature, T_t is defined as the critical temperature with the maximal magnetization on the heating curve under a magnetic field of 1 T. T_{SR} and T_C are both obtained from the extremum positions on the temperature derivative of the heating curves under a magnetic field of 0.01 T. The magnetic entropy change was calculated from the *M-T* curves using the Maxwell relations.

First-principles electronic structure calculations were performed in the framework of the density functional theory (DFT). The Vienna ab initio simulation package (VASP) [22,23] in the projector augmented wave (PAW) method [24,25] was employed to perform the DFT calculations using the generalized gradient approximation of Perdew-Burke-Ernzerhof (PBE) [26] for the exchange correlation functional. The valence electron configuration was $3p^6 3d^5 4s^2$ for Mn, $5s^2 5p^3$ for Sb and $5d^{10} 6s^2 6p^3$ for Bi. All calculations were performed for a 1⊕2⊕1 supercell. The structural degrees of freedom were fully relaxed on a gamma centered k-grid of 7⊕7⊕7. The k-space integrations were performed with the Methfessel-Paxton method [27] of second order with a smearing width of 0.05 eV. The lattice parameters and atomic positions were relaxed for a force convergence of 0.1 meV/Å, while the energies were converged to 1 μeV. The kinetic energy cutoff was set at 520 eV.

To investigate the site preference two Bi atoms were placed on various possible combinations of the crystallographic sites. The energy cost of forming each structure is calculated as the difference between energies of Bi-doped (E_{doped}) and pure (E_{pure}) compounds minus chemical potential of two Bi atoms (2 μ_{Bi}) plus the chemical

potential of the first atom *s1* and second atom *s2* that Bi substitutes for (μ_{s1} and μ_{s2}):

$$E_f = E_{doped} + \mu_{s1} + \mu_{s2} - (E_{pure} + 2\mu_{Bi}) \quad (1)$$

The chemical potentials are obtained by first optimizing the structure for each element (rhombohedral for Sb and Bi, cubic for Mn) and then taking the value of total energy per atom.

3. Results and discussion

The XRD data at room temperature in $Mn_2Sb_{1-x}Bi_x$ and the derived lattice parameters of the tetragonal lattice structure are shown in Fig. 1. The lattice parameters for the Mn_2Sb-based compound with $x = 0$ ($a = 4.077$ Å and $c = 6.543$ Å) are slightly lower than the ones reported in an earlier study ($a = 4.078$ Å and $c = 6.557$ Å) [28]. This small discrepancy can be due to deviations in the chemical composition caused by the occurrence of the typical impurity phase MnSb. As shown in Fig. 1(a), with the increase of the amount of Bi doping, additional secondary phases are detected besides the main phase of Cu_2Sb-type tetragonal Mn_2Sb. A minor impurity phase MnSb (about 5%) appears in samples with $x < 0.09$. The refined parameters and the fraction of the main impurity phase MnSb can be found in Tables S1 and S2 in the Supplementary Material. Their chemical compositions of the main phase in the $x = 0.05$ and 0.07 samples are determined to be $Mn_{68.0}Sb_{29.6}Bi_{2.4}$ and $Mn_{66.5}Sb_{31.0}Bi_{2.5}$ by EDS, which are both close to their nominal compositions $Mn_{66.7}Sb_{31.7}Bi_{1.7}$ and $Mn_{66.7}Sb_{31.0}Bi_{2.3}$, respectively. The increasing values for the lattice parameters *a* and *c* and the unit-cell volume *V* with increasing Bi concentration in Fig. 1(b) and (c) confirm the inclusion of Bi in the Mn_2Sb matrix. This trend is opposite to the reduced unit-cell volume observed in Mn_2Sb-based compounds with smaller atom substitutions such as Cr replacing Mn [8] or Sn replacing Sb [15]. The opposite trend of lattice parameters between our results and Zhang et al. [20] could be attributed to the different fractions of MnSb and occupation of Bi in Mn_2Sb. Further Bi doping ($x > 0.09$) induces multiple secondary phases: hexagonal ($P63/mmc$ symmetry) MnBi, rhombohedral (R-3m symmetry) Bi and cubic (I-43m symmetry) Mn. The insignificant evolution of the main-phase lattice parameters and unit-cell volume beyond 9% Bi concentration and the appearance of the secondary phase Bi in $x = 0.09$ suggest a solid solubility limit 7–9% of Bi in the Mn_2Sb matrix phase. The proposed solubility limit of Bi in Mn_2Sb has been indicated in Fig. 2(d) as the turning point in c/a at $x = 0.09$. The decrease in lattice parameters *a* and *c* and unit-cell volume *V* for $x = 0.20$ is attributed to deviations in the chemical composition caused by the formation of Bi-rich impurity phases.

The temperature dependent magnetization curves are shown in Fig. 2(a, b) for $x = 0.05$. The weak splitting of the ZFC and FC curves under a field of 0.01 T in Fig. 2(a) is expected to be due to the presence of the ferromagnetic (FM) impurity phase MnSb [29], which is in agreement with the XRD results. Starting at the lowest temperature with increasing temperature, the ZFC curve runs from a low value in the AFM state with spins in the *a*-*b* plane up to a temperature of about 150 K, where the magnetic transition temperature T_t of AFM-FIM is approached and a high spin alignment is observed. Then the magnetization drops dramatically at about 260 K, where the spins flip parallel along the *c* axis. This phenomenon has been reported for $(Mn_2Sb)_{0.89}Bi_{0.11}$ [19,20], and has been attributed to the spin-reorientation effect. The spin-flip transition process in the FC curve is fuzzier than in the FH and ZFC curves, which indicates that thermal history affects the spin orientation [13]. This feature smears out under stronger magnetic field, suggesting that the magnetocrystalline anisotropy is overcome by the Zeeman splitting provided by the magnetic field of 1 T [30]. The spin-orientation effect could be responsible for the larger thermal hysteresis of *M-T* curves for a field of 0.01 T compared to 1 T in Fig. 2(b).

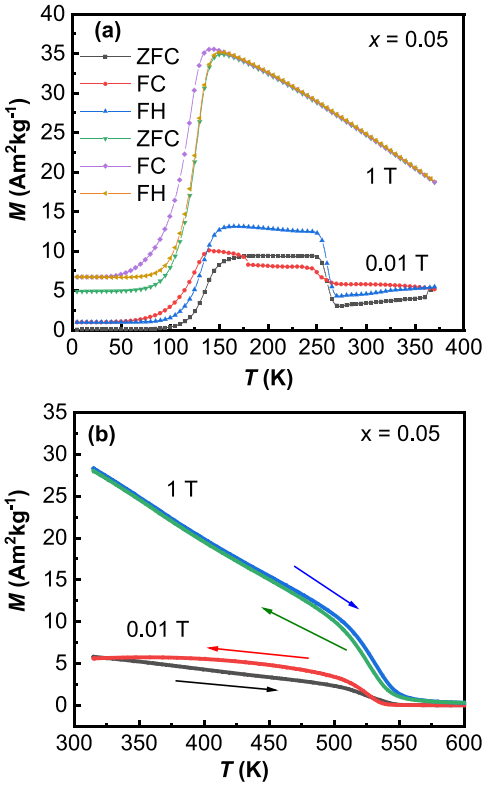

Fig. 2. (a) *M-T* curves for $Mn_2Sb_{1-x}Bi_x$ with $x = 0.05$ under magnetic fields of 0.01 and 1 T for a temperature range of 5–370 K and (b) for a temperature range of 315–600 K.

Fig. 3(a) and (b) display the *M-T* curves of $Mn_2Sb_{1-x}Bi_x$ ($x = 0$, 0.02, 0.04, 0.05, 0.07, 0.09, 0.15, 0.20) under magnetic fields of 0.01 T and 1 T, respectively. Compared with other Bi substituted Mn_2Sb compounds, the larger splitting of ZFC and FC curves in $x = 0.02$ is ascribed to the combined effects of the FM impurity phase MnSb and the incomplete FIM-AFM transition [20]. In Fig. 3(b), the magnetization of pure Mn_2Sb monotonically increases with decreasing temperature, while the magnetization of Bi-containing samples initially increases, then abruptly drops at a certain temperature, reaches a minimum and finally increases slowly with decreasing temperature. The saturation magnetization of pure Mn_2Sb is 40 Am^2/kg excluding 5 Am^2/kg from the MnSb impurity phase (estimated from the XRD data), which is in agreement with earlier studies [29,31]. It is evident that partial substitution of Sb by Bi causes the AFM-FIM transition at T_t.

Fig. 3(c) and (d) summarize the magnetization jump ΔM at the AFM-FIM transition, together with T_t, T_{SR} and T_C derived from the *M-T* curves (the definitions of these critical temperatures are given in the experimental section). The hatched area refers to the concentration range beyond Bi solubility limit. ΔM first increases with increasing Bi concentration when $x \leq 0.09$ because a large amount of Bi triggers a larger fraction of the FIM-AFM transition, which decreases the residual FIM at the AFM region. Then ΔM decreases with further Bi addition because the fraction of secondary phases increases and as the main secondary phase MnBi is ferromagnetic below 633 K, this increases the magnetization in the AFM region. The maximal ΔM (30 Am^2/kg) and the highest T_t (156 K) are both found for $x = 0.07$, beyond which Bi as one of the secondary phases appears.

According to the magnetic phase diagram for $Mn_2Sb_{1-x}Bi_x$ in Fig. 3(d), T_{SR} rises slowly for increasing Bi concentration (starting from 255 K for $x = 0.02$ and saturating at 262 K for $x = 0.09$). This trend is in line with Co substitution in Mn_2Sb [13]. T_t as the function of Bi concentration shows a comparable trend as ΔM. For increasing Bi concentration, the AFM exchange interaction between the

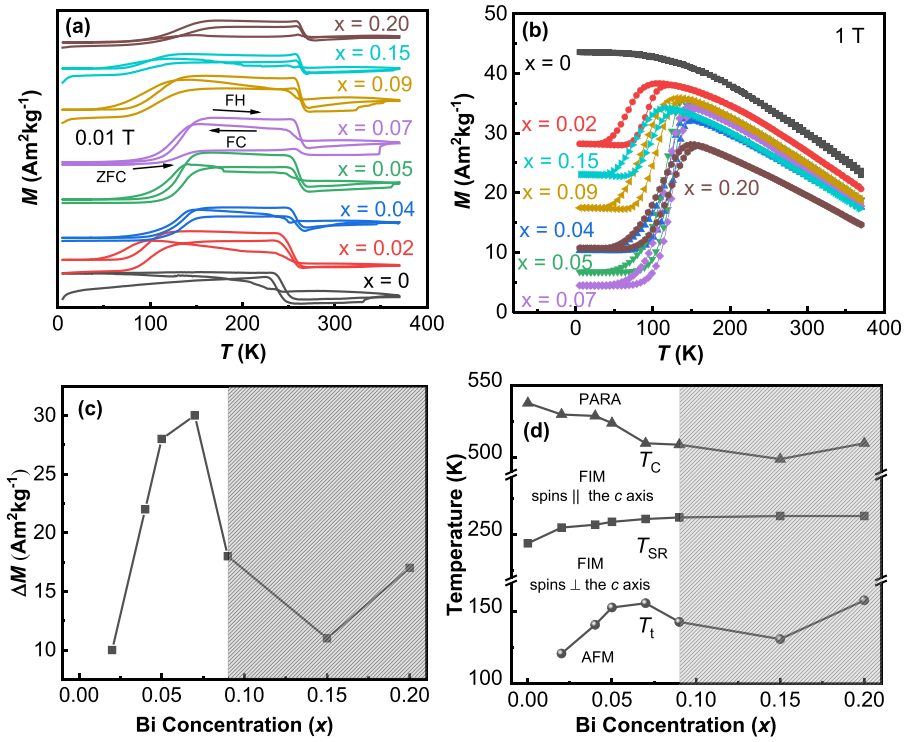

Fig. 3. (a) The temperature dependence of magnetization for $Mn_2Sb_{(1-x)}Bi_x$ (x = 0, 0.02, 0.04, 0.05, 0.07, 0.09, 0.15, 0.20) under a magnetic field of 0.01 T and (b) under a magnetic field of 1 T. (c) The maximal magnetization jump ΔM at the AFM-FIM transition obtained from heating curves under 1 T as the function of the Bi concentration. (d) Magnetic phase diagram of $Mn_2Sb_{(1-x)}Bi_x$. The hatched area refers to the range beyond the solubility limit for Bi.

Mn-I and Mn-II moments becomes stronger as a result of the decrease in the c/a ratio in Fig. 1(d), which shifts the transition to higher temperatures [32]. T_C decreases linearly with Bi concentration. The slope of the fitting curve is about −2.66 K/T within the Bi solubility limit. The T_C of pure Mn_2Sb is 538 K, which is somewhat below the 550 K reported by Wilkinson et al. [9], and this is probably associated with slightly lower lattice parameters. The deviation observed for T_t and T_C at x = 0.20 is attributed to the abnormal lattice parameters of main phase, caused by excess secondary phases (about 20% MnBi and about 10% Bi). Compared with $Mn_2(Cr)Sb$ [8], a narrower temperature window for T_t (121–156 K) and T_C (538–509 K) is presented by Bi substitution, which is probably due to larger atom size of Bi.

The magnetocaloric effect of the $Mn_2Sb_{1-x}Bi_x$ compounds has been studied by measuring isofield magnetization and subsequent application of Maxwell relations [33]. In Fig. 4(a) the M-T curves are shown for x = 0.05 upon heating in magnetic fields ranging from 0.2 to 5 T. The magnetization shows a clear jump at T_t under all magnetic fields. T_t shifts to lower temperature with increasing field as the magnetic field favours the high-temperature high-magnetization FIM state. The size of the shift in transition temperature with magnetic field is estimated to be $dT_t/d\mu_0H$ = −5.4 K/T from the data in Fig. 4(b). This value is higher than the reported value of −4.3 K/T for $Mn_{1.92}Cr_{0.08}Sb$ [8]. Since the magnetic field shifts the transition temperature to a lower temperature, which is different from the conventional MCE, the magnetocaloric effect for $Mn_2Sb_{1-x}Bi_x$ corresponds to the inverse MCE. The magnetic entropy change for the compound with x = 0.05 is shown in Fig. 4(c) and (d) for the heating and cooling curves, respectively. The magnetic entropy change is calculated based on the integrated Maxwell relation: $\Delta S(\Delta H, T) = \int_{H_0}^{H} \left(\frac{\partial M(T,H)}{\partial T}\right)_H d\mu_0 H$, where we choose $\mu_0 H_0$ = 0 T. The maximum entropy change under a field change of 5 T in the heating curves is 2.44 J/kg K at 116 K whereas in the cooling curves it is 1.91 J/kg K at 105 K. The maximum entropy change (2.44 J/kg K) is similar to the reported value of 1.97 J/kg K for $(Mn_2Sb)_{0.93}Bi_{0.07}$ by measuring isothermal field-up magnetization [20]. The temperature window for the latter (74 K) is wider than for the former (53 K). The difference in magnetic entropy change between heating and cooling is attributed to large thermal hysteresis of about 10 K, as shown in Fig. 2(a).

In order to know what position the Bi atoms prefer to occupy in the Mn_2Sb lattice, we employed spin-polarized DFT calculations for the formation energy, magnetic moment, lattice constants a and c and unit-cell volume V for a Bi concentration of x = 0.04. The results are summarized in Table 1. The calculated magnetic moments (2.3 μ_B for Mn-I and −3.4 μ_B for Mn-II) for pure Mn_2Sb are in agreement with published data (2.13 μ_B for Mn-I and −3.87 μ_B for Mn-II) measured by neutron diffraction [9]. The calculated lattice constants (a = 3.94 Å and c = 6.44 Å) are comparable with those derived from XRD. Among all studied configurations we find the lowest formation energy (also the closest cell volume and lattice constants to pure Mn_2Sb) when the Bi atoms solely occupy the Sb site. Given the low Bi concentrations involved, this result for x = 0.04 is expected to be representative for all the studied samples up to the solubility limit (x < 0.09). The substitution of the non-magnetic Sb atoms by Bi atoms leads to a decrease in the atomic magnetic moment for Mn-I and an increase for Mn-II. A comparable magnetization is expected when Bi preferentially replaces non-magnetic Sb. This agrees with the following experimental results: the magnetization jump at the AFM-FIM is according to Fig. 2(a) equal to 12 Am^2/kg under a field of 0.01 T, which is larger than the 4 Am^2/kg for $Mn_{2-x}Cr_xSb$ compounds under a field of 0.02 T [8], where the Cr atoms occupy the Mn-I site [34].

The exchange inversion proposed by Kittel [18] was initially used to describe the AFM-FIM transition in $Mn_{2-x}Cr_xSb$. The sign of the exchange interaction will change when the lattice parameter go across a critical value at the critical temperature. This can occur as a result of the normal expansion or contraction of the materials with temperature. For pure Mn_2Sb, the normal thermal contraction is not sufficient to trigger the

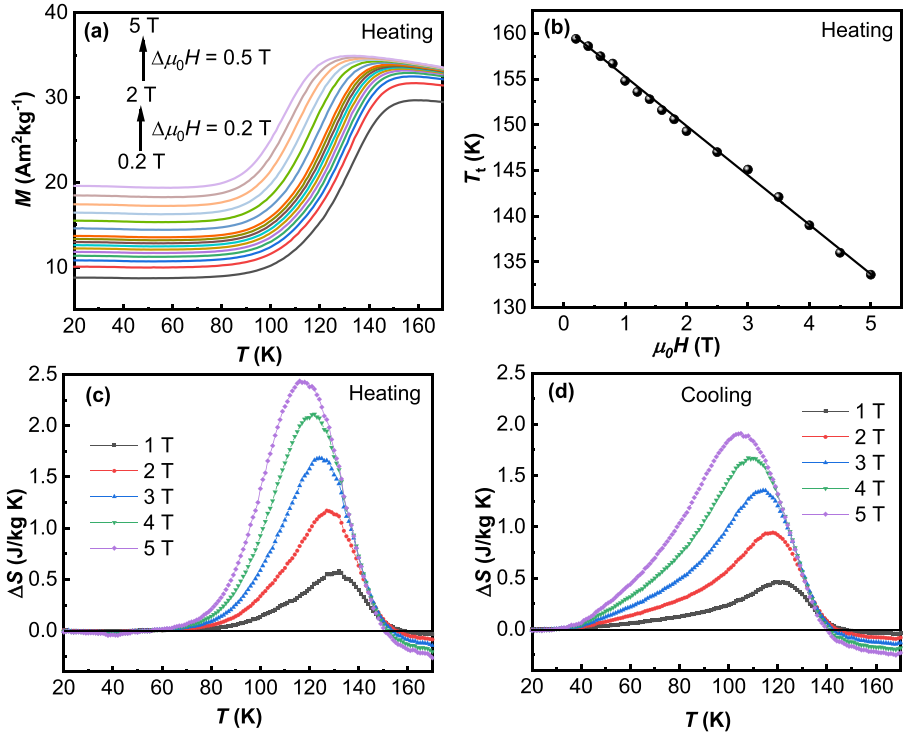

Fig. 4. (a) *M-T* curves for $Mn_2Sb_{(1-x)}Bi_x$ with $x = 0.05$ for heating in different applied magnetic fields. (b) T_t as a function of magnetic field. The magnetic entropy change ΔS calculated from the (c) heating curves and (d) cooling curves.

Table 1
Volume *V*, lattice constants *a* and *c*, formation energy E_f, magnetic moment on the constituent atoms Mn-I and Mn-II per formula unit of $Mn_2Sb_{0.96}Bi_{0.04}$.

Occ (Bi)	E_f (eV)	Mn-I (μ_B)	Mn-II (μ_B)	V (Å^3)	a (Å)	c (Å)
Mn-I	0.69	3.0	-3.5	113.7	3.90	7.15
Mn-I Mn-II	0.51	2.8	-3.4	116.8	4.16	6.55
Mn-I Sb	0.54	2.7	-3.5	109.6	4.01	6.81
Mn-II	0.26	2.9	-3.8	118.0	4.26	6.51
Mn-II Sb	-0.21	2.4	-3.6	108.2	4.08	6.51
Sb	-0.47	1.9	-3.5	101.7	4.00	6.37
None	-1.38	2.3	-3.4	99.9	3.94	6.44

exchange inversion, but the exchange inversion becomes accessible with the help of chemical compression [15] by substitution with smaller atoms such as Cr replacing Mn [8], Sn replacing Sb [15]. Besides, the critical temperature could be reached by the enhanced coefficient of thermal expansion along the *c* axis, which affects the temperature dependent interatomic distances. As a larger Mn-Mn interatomic distance for Bi substituted Mn_2Sb is inferred from the larger lattice parameters at room temperature, the origin of the AFM-FIM transition in $Mn_2Sb_{1-x}Bi_x$ is ascribed to an enhancement of the coefficient of thermal expansion along the *c* axis by Bi substitution [35]. To verify this assumption, the thermal expansion coefficient was investigated in $x = 0.07$ by variable temperature XRD in the temperature range of 298–698 K. The coefficient for $x = 0.07$ ($x = 0.05$) are 2.0×10^{-5} K^{-1} (1.9×10^{-5} K^{-1}) along the *c* axis at room temperature, which is higher than the value (1.4×10^{-5} K^{-1}) reported by Heaton et al. [28]. The counterpart along the *a* axis is 2.3×10^{-5} K^{-1} (2.2×10^{-5} K^{-1}), which is lower than the values (4.0×10^{-5} K^{-1}) reported by Heaton et al. [28]. Bi substitution thus affects the environment around the Mn atoms and stabilizes antiferromagnetism [16].

4. Conclusions

In summary, the structure and magnetic properties of $Mn_2Sb_{1-x}Bi_x$ ($x = 0$, 0.02, 0.04, 0.05, 0.07, 0.09, 0.15, 0.20) have been investigated. It is observed that Bi substitution for Sb causes an increase in lattice parameters, a large magnetization jump identified as the AFM-FIM transition and an impressive magnetic field dependence of transition temperature of $dT_t/d\mu_0 H = -5.4$ K/T. The transition temperature and magnetization jump both increase with increasing Bi concentration up to a value of $x = 0.09$, which is found to be the solubility limit of Bi. The exchange inversion in $Mn_2Sb_{1-x}Bi_x$ caused by the substitution with a larger atom is ascribed to the enhanced coefficient of thermal expansion along the *c* axis, the stacking direction of the Mn-I and Mn-II layers.

CRediT authorship contribution statement

Qi Shen: Conceptualization, Methodology, Validation, Formal analysis, Investigation, Visualization, Writing - original draft. **Ivan Batashev**: Formal analysis, Software, Writing - review & editing. **Fengqi Zhang**: Formal analysis, Investigation. **Hamutu Ojiyed**: Investigation. **Niels van Dijk**: Supervision, Writing - reviewing & editing. **Ekkes Brück**: Supervision, Writing - reviewing & editing.

Declaration of Competing Interest

The authors declare that they have no known competing financial interests or personal relationships that could have appeared to influence the work reported in this paper.

Acknowledgements

This work is part of the project 'Energy Conversion with Highly Responsive Magnetic Materials for Efficiency' funded by Dutch Research Council with Poject No. 680-91-013 and co-financed by Swiss Blue Energy and RSP Technology. The authors acknowledge the technical help provided by A.J.E. Lefering. Qi Shen would like to thank Xuefei Miao for his assistance with the XRD refinement.

Appendix A. Supporting information

Supplementary data associated with this article can be found in the online version at doi:10.1016/j.jallcom.2021.158963.

References

[1] O. Gutfleisch, M.A. Willard, E. Brück, C.H. Chen, S.G. Sankar, J.P. Liu, Magnetic materials and devices for the 21st century: stronger, lighter, and more energy efficient, Adv. Mater. 23 (2011) 821–842.
[2] S.M. Sandoval, K.P. Wetzlar, G.P. Carman, Thermomagnetic conversion efficiencies for ferromagnetic materials, J. Appl. Phys. 110 (2011) 123923.
[3] V.K. Pecharsky, K.A. Gschneidner, Giant magnetocaloric effect inGd5(Si2Ge2), Phys. Rev. Lett. 78 (1997) 4494–4497.
[4] H. Wada, Y. Tanabe, Giant magnetocaloric effect of MnAs1−xSbx, Appl. Phys. Lett. 79 (2001) 3302–3304.
[5] T. Krenke, E. Duman, M. Acet, E.F. Wassermann, X. Moya, L. Manosa, A. Planes, Inverse magnetocaloric effect in ferromagnetic Ni–Mn–Sn alloys, Nat. Mater. 4 (2005) 450–454.
[6] F. Hu, B. Shen, J. Sun, Z. Cheng, G. Rao, X. Zhang, Influence of negative lattice expansion and metamagnetic transition on magnetic entropy change in the compound LaFe11.4Si1.6, Appl. Phys. Lett. 78 (2001) 3675–3677.
[7] O. Tegus, E. Brück, K.H.J. Buschow, F.R. Boer, Transition-metal-based magnetic refrigerants for room-temperature applications, Nature 415 (2002) 150–152.
[8] L. Caron, X. Miao, J.C.P. Klaasse, S. Gama, E. Brück, Tuning the giant inverse magnetocaloric effect in Mn2−xCrxSb compounds, Appl. Phys. Lett. 103 (2013) 112404.
[9] M.K. Wilkinson, N.S. Gingrich, C.G. Shull, The magnetic structure of Mn2Sb, J. Phys. Chem. Solids 2 (1957) 289–300.
[10] W.H. Cloud, H.S. Jarrett, A.E. Austin, E. Adelson, Neutron diffraction studies of chromium-modified Mn2Sb, Phys. Rev. 120 (1960) 1969–1970.
[11] W. Cui, W. Ren, Z. Zhang, X. Zhou, H. Zhong, Q. Wang, Lattice distortion tuning of the metamagnetic phase transition in tetragonal Cu2Sb-type Mn1.95V0.05Sb alloy, Scr. Mater. 143 (2018) 59–62.
[12] S. Ohta, Y. Hasebe, T. Kanomata, T. Kanek, Thermal expansion and magnetic properties of Mn2−xZnxSb, J. Magn. Magn. Mater. 104–107 (1992) 1979–1980.
[13] J. Wilden, A. Hoser, M. Chikovani, J. Perßon, J. Voigt, K. Friese, A. Grzechnik, Magnetic transitions in the Co-modified Mn2Sb system, Inorganics 6 (2018) 113.
[14] J. Zhang, G. Yao, S. Chen, F. Wei, X. Fan, X. Yin, Z. Chen, W. Cui, Q. Wang, The effects of Ge occupation and hydrostatic pressure on the metamagnetic phase transition and magnetocaloric effect in Mn2Sb alloy, AIP Adv. 9 (2019) 035106.
[15] V.M. Ryzhkovskii, V.P. Dymont, Z.L. Erofeen, Ferromagnetic-a ntiferromagnetic phase transition in Mn2Sb(Sn) solid solutions, Phys. Stat. Sol. (a) 130 (1992) 163–168.
[16] T. Kakimoto, J. Goto, S. Fujii, K. Koyama, S. Ishida, Electronic and magnetic properties of $Mn_2Sb_{1-x}As_x$ (x = 0,0.5,1), Mater. Trans. 55 (2014) 1878–1884.
[17] L. Caron, Chapter 3, Handbook of Magnetic Materials, first ed., 29 Elsevier, 2020.
[18] C. Kittel, Model of exchange-inversion magnetization, Phys. Rev. 120 (1960) 335–342.
[19] S. Ohshima, K. Fukamichi, T. Wakiyama, T. Anayama, Magnetic first-order phase transition in Bi-modified Mn2Sb, Jpn. J. Appl. Phys. 18 (1979) 707–708.
[20] Z. Zhang, Y. Zhang, X. Luo, S. Ma, H. Zeng, G. Yu, X. Zheng, C. Chen, Y. Hu, F. Xu, S.U. Rehman, Z. Zhong, Self-organized Bi-rich grain boundary precipitates for realizing steep magnetic-field-driven metamagnetic transition in Bi-doped Mn2Sb, Acta Mater. 200 (2020) 835–847.
[21] B.H. Toby, Rfactors in Rietveld analysis: how good is good enough, Powder Diffr. 21 (2006) 67–70.
[22] G. Kresse, J. Hafner, Ab initiomolecular dynamics for liquid metals, Phys. Rev. B 47 (1993) 558–561.
[23] G. Kresse, J. Furthmüller, Efficiency of ab-initio total energy calculations for metals and semiconductors using a plane-wave basis set, Comput. Mater. Sci. 6 (1996) 15–50.
[24] P.E. Blöchl, Projector augmented-wave method, Phys. Rev. B 50 (1994) 17953–17979.
[25] G. Kresse, D. Joubert, From ultrasoft pseudopotentials to the projector augmented-wave method, Phys. Rev. B 59 (1999) 1758–1775.
[26] J.P. Perdew, K. Burke, M. Ernzerhof, Generalized gradient approximation made simple, Phys. Rev. Lett. 77 (1996) 3865–3868.
[27] M. Methfessel, A.T. Paxton, High-precision sampling for Brillouin-zone integration in metals, Phys. Rev. B 40 (1989) 3616–3621.
[28] L. Heaton, N.S. Gingrich, The crystal structure of Mn2Sb, Acta Cryst. 8 (1955) 207–210.
[29] A. Tekgül, Ö. Çakır, M. Acet, M. Farle, N. Ünal, The structural, magnetic, and magnetocaloric properties of In-doped Mn2−xCrxSb, J. Appl. Phys. 118 (2015) 153903.
[30] Y. Cao, K. Xu, Z. Li, Y. Zhang, X. He, Y. Kang, W. Sun, T. Gao, Z. Qian, C. Liu, M. Ye, C. Jing, Interplay between spin reorientation and magnetoelastic transitions, and anisotropic magnetostriction in the Mn1.95Cr0.05Sb single crystal, J. Magn. Magn. Mater. 487 (2019) 165315.
[31] F.J. Darnell, W.H. Cloud, H.S. Jarrett, X-ray and magnetization studies of Cr-modified Mn2Sb, Phys. Rev. 130 (1963) 647–655.
[32] Y. Zhang, Z. Zhang, Metamagnetic-transition-induced giant magnetoresistance in Mn2Sb1−xSnx($0 < x < \sim 0.4$) compounds, Phys. Rev. B 67 (2003) 132405.
[33] L. Caron, Z. Ou, T.T. Nguyen, D.T. Cam Thanh, O. Tegus, E. Brück, On the determination of the magnetic entropy change in materials with first-order transitions, J. Magn. Magn. Mater. 321 (2009) 3559–3566.
[34] A.E. Austin, E. Adelson, W.H. Cloud, Magnetic structures of chromium-modified Mn2Sb, Phys. Rev. 131 (1963) 1511–1517.
[35] K. Shirakawa, H. Ido, Magnetic transition of intermetallic compounds $Mn_2Sb_{(1-x)}Bi_x$ ($0 \le x \le 0.175$) with Cu_2Sb type structure, J. Jpn. Inst. Met. 43 (1979) 636–639.